Peak in the far-infrared conductivity of strongly anisotropic cuprates

A. Pimenov,[1] A. V. Pronin,[1,*] A. Loidl,[1] A. Tsukada,[2] and M. Naito[2]
[1]*Experimentalphysik V, Elektronische Korrelationen und Magnetismus, Institut für Physik, Universität Augsburg, 86135 Augsburg, Germany*
[2]*NTT Basic Research Laboratories, 3-1, Morinosato-Wakamiya, Atsugi-shi, Kanagawa 243-0198, Japan*
(Received 1 July 2002; published 31 December 2002)

We investigate the far-infrared and submillimeter-wave conductivity of electron-doped $La_{2-x}Ce_xCuO_4$ tilted 1° off from the *ab*-plane. The effective conductivity measured for this tilt angle reveals an intensive peak in the normal-state at finite frequency ($\nu \sim 50$ cm^{-1}) due to a mixing of the in-plane and out-of-plane responses. The peak disappears for the pure in-plane response and transforms into a pure Drude-like contribution. A comparative analysis of the mixed and the in-plane spectra allows us to extract the *c*-axis conductivity which shows a Josephson plasma resonance at $\nu \simeq 11.7$ cm^{-1} in the superconducting state.

DOI: 10.1103/PhysRevB.66.212508 PACS number(s): 74.25.Gz, 74.76.−w

Far-infrared conductivity in the normally conducting state of the high-T_c cuprates can be well characterized by a Drude-like response.[1] This response leads to the leveling off of the real part of the conductivity $\sigma^* = \sigma_1 + i\sigma_2$ in the submillimeter frequency range.[2,3] In some cases deviations from this behavior can be observed in the conductivity spectra as broad maxima at far-infrared frequencies. One possible reason for such an additional excitation can be a charge localization induced by doping.[4] More generally, disorder, such as an inhomogeneous oxygen distribution,[5–7] has been shown to lead to a an additional maximum in the conductivity.[8] Further possible effects leading to a conductivity peak include charge density waves[9] or reduced dimensionality in the static stripe phase.[10]

In this paper we present another possible mechanism for a finite-frequency peak in the infrared conductivity of electron-doped cuprate $La_{2-x}Ce_xCuO_4$ (LCCO). The same arguments will hold for all strongly anisotropic, mostly two-dimensional metals in which the out-of-plane response is nearly insulating. In the present case the peak arises from a small admixture of the *c*-axis response to the in-plane conductivity. Rotating the polarization of the infrared radiation, the pure in-plane response can also be measured. The in-plane conductivity shows no infrared peak but follows the predictions of the Drude model. The comparative analysis of the spectra for different experimental geometries allowed to extract conductivity and dielectric constant along the *c* axis. We note that similar effects have been described for the case of polycrystalline $YBa_2Cu_3O_{7-y}$ and at higher frequencies by Orenstein and Rapkine.[11] The polycrystalline character of the samples resulted in a homogeneous distribution of all tilt angles and led to the extrinsic conductivity peak around 1 eV. The effects described in Ref. 11 and in the present contribution rely on the strong anisotropy of the sample and disappear in the isotropic case.

A $La_{2-x}Ce_xCuO_4$ film with $x = 0.081$ was deposited by molecular-beam epitaxy[12,13] on a transparent $SrLaAlO_4$ substrate, $10 \times 10 \times 0.5$ mm^3 in size. The thickness of the film was 140 nm and the film revealed a sharp transition ($\Delta T_c < 1$ K) at 25 K. As can be deduced from the low Ce concentration, the sample belongs to the underdoped regime and hence, the transition temperature is lower than in optimally doped compounds ($T_c = 30$ K).[13] The $SrLaAlO_4$ substrate has been cut close to the (001) K direction with the misfit angle of $\alpha = 1° \pm 0.1°$. In this case the film grows nearly *c* axis oriented with the same off-axis tilt angle.

In order to obtain the complex conductivity in the frequency range from submillimeter to far-infrared wavelengths, two different experimental methods[14] have been applied to the same film. For frequencies below 40 cm^{-1} the complex conductivity of the film has been obtained by the submillimeter transmission spectroscopy.[15] At higher frequencies the reflectance has been measured using standard far-infrared techniques and the conductivity was obtained via a Kramers-Kronig analysis of the spectra. The transmission experiments for frequencies 5 cm$^{-1} < \nu < 40$ cm^{-1} were carried out in a Mach-Zehnder interferometer arrangement[15] which allows both measurements of the transmittance and the phase shift of a film on a substrate. The properties of the blank substrate were determined in a separate experiment. Utilizing the Fresnel optical formulas for the complex transmission coefficient of the substrate-film system, the absolute values of the complex conductivity $\sigma^* = \sigma_1 + i\sigma_2$ were determined directly from the measured spectra. In the frequency range $40 < \nu < 4000$ cm^{-1} reflectivity measurements were performed using a Bruker IFS-113v Fourier-transform spectrometer. In addition, the reflectance for frequencies $5 < \nu < 40$ cm^{-1} has been calculated from the complex conductivity data of the same sample, obtained by the submillimeter transmission. This substantially improves the quality of the subsequent Kramers-Kronig analysis of the reflectance and therefore the reliability of the data at the low-frequency part of the infrared spectrum.

Due to the tilt structure of the film, two main experimental geometries are possible. Both cases are depicted in Fig. 1. In the first case (upper drawing) the currents, induced by the incident radiation, are within the CuO_2 plains only. Therefore, the pure in-plane response is obtained in this case. In the other experimental geometry (lower drawing in Fig. 1) a small admixture of the *c*-axis response is expected.

Figure 1 shows the far-infrared reflectance of the LCCO film for both possible experimental geometries. Sharp structures above 200 cm^{-1} are attributed to the phonons in the

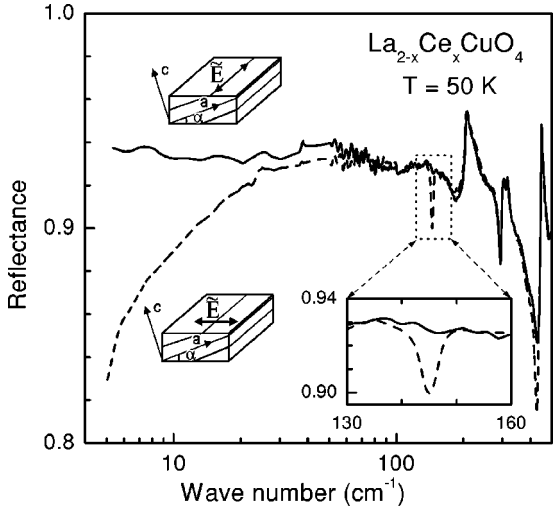

FIG. 1. Far-infrared reflectance of an underdoped LCCO film at different experimental geometries at $T=50$ K (normal-state). Solid lines: pure in-plane response, dashed lines: tilted geometry. The reflectance data above 40 cm^{-1} were measured directly and the spectra below this frequency were calculated from the complex conductivity data obtained by the transmittance technique. The inset shows the magnified spectra around a longitudinal *c*-axis phonon.

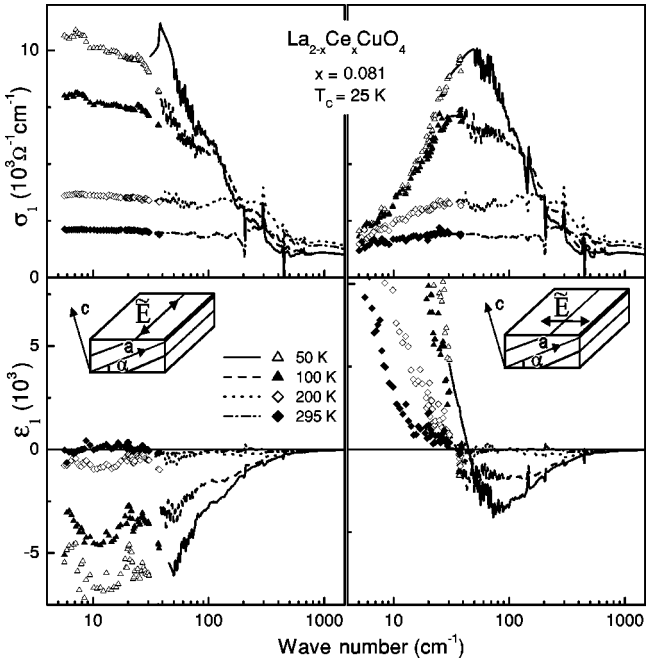

FIG. 2. Far-infrared conductivity of LCCO film in the normal state for two different experimental geometries as indicated in the insets. Upper panels: σ_1, lower panels: $\varepsilon_1=-\sigma_2/\omega\varepsilon_0$. Left panels: in-plane response, right panels: mixed ac geometry. Lines represent the results obtained from the infrared reflectance and symbols represent the data as measured directly by the submillimeter transmission technique.

substrate. In that case no substantial difference is seen between the reflectance in both geometries. In addition to these effects, sharp minima in reflectance can be observed, which reveal a clear polarization dependence. One of these resonances is shown in the inset. We interpret these resonances as LO phonons in LCCO. The eigenfrequencies (145, 427, and 553 cm^{-1}) are close to the frequencies of the out-of-plane LO phonons in $Nd_{2-x}Ce_xCuO_4$ (144, 433, and 559 cm^{-1}).[16] The most important difference between the spectra of two experimental geometries is seen below 50 cm^{-1}: the spectra of the mixed geometry deviate significantly for decreasing frequencies.

The reflectivity of a thin metallic film on a dielectric substrate can be obtained from the Maxwell equations[17]

$$r=\frac{r_{0f}+r_{fs}\exp(4\pi i n_f d/\lambda)}{1+r_{0f}r_{fs}\exp(4\pi i n_f d/\lambda)}, \qquad (1)$$

where $r_{0f}=(1-n_f)/(1+n_f)$ and $r_{fs}=(n_f-n_s)/(n_f+n_s)$ are the Fresnel reflection coefficients at the air-film (r_{0f}) and film-substrate (r_{fs}) interfaces. Here $n_f=(i\sigma^*/\varepsilon_0\omega)^{1/2}$ and n_s are the complex refractive indices of the film and substrate, respectively, λ is the radiation wavelength, d is the film thickness, $\omega=2\pi\nu$ is the angular frequency, $\sigma^*=\sigma_1+i\sigma_2$ is the complex conductivity of the film, and ε_0 is the permittivity of free space. Equation (1) is written neglecting the multiple reflections from the opposite sides of the substrate. If the film thickness is smaller than the penetration depth ($|n_f|d\ll\lambda$) and if $|n_f|\gg|n_s|$, Eq. (1) can be simplified to

$$r\approx\frac{1-\sigma^* dZ_0-n_s}{1+\sigma^* dZ_0+n_s}, \qquad (2)$$

where $Z_0=\sqrt{\mu_0/\varepsilon_0}\simeq 377\Omega$ is the impedance of free space.

Figure 2 shows the far-infrared conductivity σ_1 and the dielectric constant $\varepsilon_1=-\sigma_2/\omega\varepsilon_0$ of LCCO in the normal state. The results above 40 cm^{-1} were obtained applying the Kramers-Kronig analysis to the reflectivity data and solving Eq. (1). Below 40 cm^{-1} the complex conductivity was calculated directly from the transmittance and phase shift. The in-plane response (left panels) resembles well the predictions of the Drude model. At low frequencies, σ_1 and ε_1 are frequency independent and ε_1 is negative. For frequencies close to the value of the scattering rate $\nu\simeq 1/2\pi\tau$, σ_1 starts to decrease and ε_1 approaches zero. On the contrary, the 1° tilted geometry (right panels) reveals dramatic changes compared to the in-plane response. The real part of the conductivity shows an intensive peak in the far-infrared range and ε_1 crosses zero becoming large and positive. Figure 2 demonstrates that already 1° off-axis geometry significantly modifies the low-frequency conductivity spectra. However, we note that the most significant changes appear in the low-frequency range, $\nu<100$ cm^{-1}. The high-frequency response of the tilted geometry approximately follows the spectra of the CuO_2 planes.

In order to understand the off-axis response we utilize a model which takes the tilted geometry of the experiment into account.[3,18] The effective conductivity of a thin film tilt by an angle α reads

$$\sigma_{\text{eff}}=\frac{-i\varepsilon_0\omega(\sigma_a\cos^2\alpha+\sigma_c\sin^2\alpha)+\sigma_a\sigma_c}{-i\varepsilon_0\omega+\sigma_a\sin^2\alpha+\sigma_c\cos^2\alpha}. \qquad (3)$$

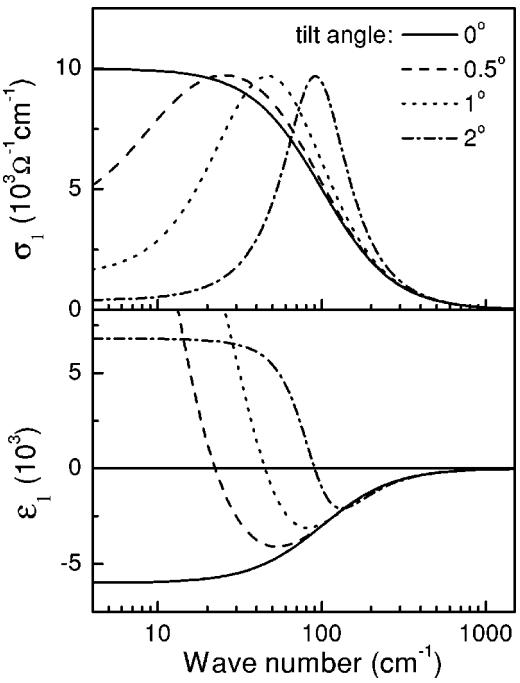

FIG. 3. Far-infrared conductivity and dielectric constant of a tilt anisotropic sample as calculated from Eq. (3). The in-plane conductivity was assumed to obey the Drude form with $\sigma_0 = 10^4\ \Omega^{-1}\,\mathrm{cm}^{-1}$, $1/2\pi\tau = 100\ \mathrm{cm}^{-1}$, and the *c*-axis response was taken as $\sigma_{1,c} = 0.5\ \Omega^{-1}\,\mathrm{cm}^{-1}$ and $\varepsilon_{1,c} = 8$.

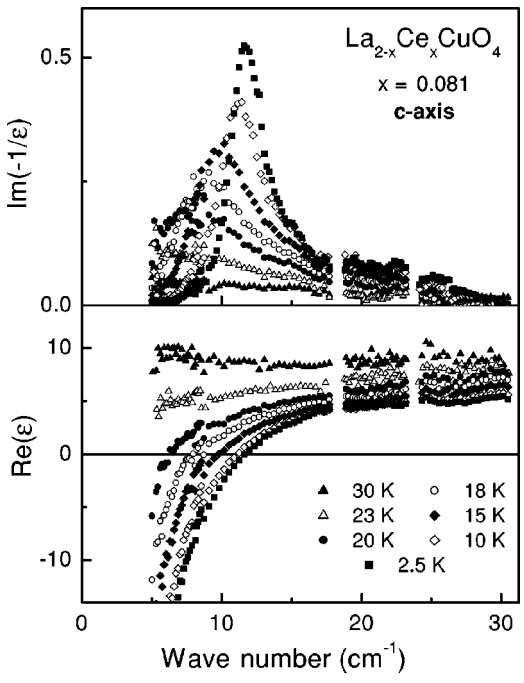

FIG. 4. Dielectric loss function and dielectric permittivity of LCCO along the *c* axis. The peak in the loss function corresponds to the Josephson plasma resonance.

Here σ_a and σ_c are the complex conductivities in the CuO_2 planes and along the *c* axis, respectively. Within the approximation $\alpha \approx \sin\alpha \ll 1$ and $|\sigma_a| \gg |\sigma_c|$, Eq. (3) can be rewritten as

$$\frac{1}{\sigma_{\mathrm{eff}}} = \frac{\alpha^2}{\sigma_c - i\varepsilon_0\omega} + \frac{1}{\sigma_a}. \tag{4}$$

It has to be noted that the tilting of the sample has a much stronger effect on the reflectance compared to experiments with oblique incidence. In the latter case the mixture of the in-plane and *c*-axis properties can be also observed,[19] but the strongest effects are produced within the grazing incidence geometry.[20] In the case of oblique incidence the effective dielectric function may be written as[20]

$$\varepsilon_{\mathrm{eff}} = \varepsilon_a \cos^2(\theta)/\sqrt{1 - \sin^2(\theta)/\varepsilon_c}, \tag{5}$$

which for small angles of incidence θ and for the *c*-axis dielectric function $|\varepsilon_c| \gg 1$ can in the first approximation be written as

$$\varepsilon_{\mathrm{eff}} \simeq \varepsilon_a(1 - \theta^2). \tag{6}$$

Here ε_a is the in-plane dielectric function. The last expression is only weakly angle dependent except for the grazing incidence.

On the contrary, for the tilted sample geometry the angular dependence of the electrodynamic parameter is much stronger. For tilt angles as small as $\alpha^2 \ll |\varepsilon_c/\varepsilon_a| \ll 1$ and neglecting in Eq. (4) the term $i\varepsilon_0\omega$ compared to σ_c, Eq. (4) can be rewritten as

$$\varepsilon_{\mathrm{eff}} = \frac{i\sigma_{\mathrm{eff}}}{\varepsilon_0\omega} \simeq \varepsilon_a\left(1 - \alpha^2\frac{\varepsilon_a}{\varepsilon_c}\right), \tag{7}$$

which is much more angle dependent compared to Eq. (6) due to the ratio $\varepsilon_a/\varepsilon_c \gg 1$.

To understand the spectra in Fig. 2 qualitatively, the *c*-axis response of LCCO can be taken as purely insulating with a dielectric constant $\varepsilon_c \simeq 10$. In that case $\sigma_c \simeq -i\varepsilon_c\varepsilon_0\omega$ and the first term in Eq. (4) dominates the response for the tilted geometry below $\omega/2\pi \simeq \sigma_a\alpha^2/(\varepsilon_c\varepsilon_0) \simeq 20\ \mathrm{cm}^{-1}$, which roughly corresponds to the conductivity maximum in the right upper panel of Fig. 2.

Figure 3 shows the conductivity and dielectric constant of a tilted sample as calculated on the basis of Eq. (3) and for different tilt angles α. The parameters of the model have been taken to correspond to the $T = 50$ K data in Fig. 2. The in-plane conductivity was assumed to obey the Drude form $\sigma^* = \sigma_0/(1 - i\omega\tau)$ with $\sigma_0 = 10^4\Omega^{-1}\,\mathrm{cm}^{-1}$, $1/2\pi\tau = 100\ \mathrm{cm}^{-1}$, and the c-axis response was taken as $\sigma_{1,c} = 0.5\ \Omega^{-1}\,\mathrm{cm}^{-1}$ and $\varepsilon_{1,c} = 8$ (i.e., $\sigma_c = \sigma_{1,c} - i\omega\varepsilon_0\varepsilon_{1,c}$). Evidently, the solid curve ($\alpha = 0$) represents the Drude response and closely resembles the in-plane conductivity of Fig. 2 (left panels, $T = 50$ K). Already for small tilt angles the effective conductivity reveals a pronounced peak in the real part of the conductivity, which for $\alpha = 1°$ shows the same shape as the spectra in the right panels of Fig. 2. Only one sample with $\alpha = 1°$ has been investigated in the present work because tilt samples are difficult to grow. However, the effective tilt angle can be varied using the same sample via different polarizations of the incident radiation. This possibility has been demonstrated previously on a tilt $Nd_{2-x}Ce_xCuO_4$ film.[18]

Comparative analysis of the in-plane and the mixed response allows us to extract the *c*-axis conductivity of LCCO inverting Eq. (3). Because the spectra for both orientations show only weak deviations at high frequencies, this procedure reveals reliable data below $\nu \sim 30\ \mathrm{cm}^{-1}$ only. The *c*-axis response of LCCO, obtained in this way, is shown in Fig. 4. The dielectric permittivity above T_c is approximately frequency and temperature independent with $\varepsilon_1 \simeq 8$ and $\sigma_1 \simeq 0.5\ \Omega^{-1}\,\mathrm{cm}^{-1}$. An additional contribution to ε_1 due to the superconducting condensate, which is proportional to $-c^2/(\omega\lambda)^2$, starts to grow below T_c. Here λ is the temperature-dependent *c*-axis penetration depth, which attains the value of $\lambda = 48\ \mu$ for $T \to 0$. Correspondingly, a zero crossing of the dielectric constant is observed in the submillimeter frequency range, which represents a Josephson plasma resonance. This resonance is most clearly seen in $\mathrm{Im}(-1/\varepsilon^*)$ as a sharp maximum close to $\nu \simeq 11.7\ \mathrm{cm}^{-1}$.

In conclusion, we presented the submillimeter-wave and far-infrared conductivity of a $La_{2-x}Ce_xCuO_4$ film measured in a tilted geometry. A broad maximum in the far-infrared conductivity can be observed within this geometry and is attributed to the admixing of the c-axis response to the in-plane conductivity. The same effects can be expected for strongly anisotropic metals, where highly conducting response along one optical axis coexists with almost insulating behavior for another direction. In addition, from the analysis of the mixed and the in-plane contributions the pure *c*-axis properties of LCCO can be extracted from the spectra, which show a Josephson plasma resonance in the superconducting state.

This work was supported by BMBF (13N6917/0-EKM).

*Permanent address: General Physics Institute of the Russian Acad. of Sciences, 119991 Moscow, Russia.

[1] D. B. Tanner and T. Timusk, in *Physical Properties of High Temperature Superconductors III*, edited by D. M. Ginsberg (World Scientific, Singapore, 1992), p. 363.
[2] A. Pimenov *et al.*, Phys. Rev. B **61**, 7039 (2000).
[3] A. Pimenov *et al.*, Phys. Rev. B **62**, 9822 (2000).
[4] D. N. Basov, B. Dabrowski, and T. Timusk, Phys. Rev. Lett. **81**, 2132 (1998).
[5] J. J. McGuire *et al.*, Phys. Rev. B **62**, 8711 (2000).
[6] A. V. Puchkov *et al.* Phys. Rev. B **51**, 3312 (1995).
[7] E. J. Singley *et al.*, Phys. Rev. B **64**, 224503 (2001).
[8] W. A. Atkinson and P. J. Hirschfeld, Phys. Rev. Lett. **88**, 187003 (2002).
[9] C. Bernhard *et al.*, Solid State Commun. **121**, 93 (2002).
[10] M. Dumm *et al.*, Phys. Rev. Lett. **88**, 147003 (2002).
[11] J. Orenstein and D. H. Rapkine, Phys. Rev. Lett. **60**, 968 (1988).
[12] M. Naito and M. Hepp, Jpn. J. Appl. Phys. **39**, L485 (2000).
[13] M. Naito and M. Hepp, Physica C **357-360**, 333 (2001).
[14] A. Pimenov, A. Loidl and S. I. Krasnosvobodtsev, Phys. Rev. B **65**, 172502 (2002).
[15] G. V. Kozlov and A. A. Volkov, in *Millimeter and Submillimeter Wave Spectroscopy of Solids*, edited by G. Grüner (Springer, Berlin, 1998), p. 51.
[16] E. T. Heyen *et al.*, Solid State Commun. **74**, 1299 (1990).
[17] O. S. Heavens, *Optical Properties of Thin Solid Films* (Dover, New York, 1991).
[18] A. Pimenov *et al.*, Appl. Phys. Lett. **77**, 429 (2000).
[19] D. van der Marel *et al.*, Phys. Rev. Lett. **71**, 2676 (1993).
[20] J. Schützmann *et al.*, Phys. Rev. B **55**, 11 118 (1997); A. A. Tsvetkov *et al.*, *ibid.* **60**, 13 196 (1999).